Materials Today xxx (xxxx) xxx

Contents lists available at ScienceDirect

Materials Today

journal homepage: www.elsevier.com/locate/mattod

Fluorinated lipid nanoparticle-mediated mRNA delivery enables high-fidelity base editing for therapeutic reversal of hereditary tyrosinemia☆

Jia Lv [a,1], Lei Yang [b,1], Xi Chen [c,1], Jin Zhang [a], Zhan Li [d], Jianan Duan [a], Tianai Zhang [a], Yiwen Li [d], Dali Li [a,*], Yiyun Cheng [a,e,*]

[a] Shanghai Frontiers Science Center of Genome Editing and Cell Therapy, Shanghai Key Laboratory of Regulatory Biology, School of Life Sciences, East China Normal University, Shanghai 200241, China
[b] Hangzhou Institute of Medicine (HIM), Chinese Academy of Sciences, Hangzhou 310018, China
[c] BRL Medicine Inc., Shanghai 201109, China
[d] College of Polymer Science and Engineering, National Key Laboratory of Advanced Polymer Materials, Sichuan University, Chengdu 610065, China
[e] Fengxian Hospital Affiliated to Southern Medical University, Shanghai 201499, China

A B S T R A C T

Intracellular delivery of base editors shows great promise for the treatment of genetic diseases caused by single-base mutations. While lipid nanoparticles (LNPs) represent a promising non-viral system for delivering single-base editor mRNA, the efficacy has been limited by inefficient endosomal escape and instability. To address these challenges, we engineered a fluorolipid-enhanced LNP system that synergizes fluorolipid-mediated endosomal escape with high nanoparticle stability. The optimized formulation demonstrated a significant improvement in the delivery of mRNA to the liver compared to conventional LNPs. Capitalizing on this system, we delivered haA3A-CBE-VA mRNA, a high-fidelity base editor optimized for methylated and GC-rich genomic regions to correct the pathogenic A-to-G mutation at the start codon of Fah in a hereditary tyrosinemia type I mouse model. This intervention restored functional Fah protein expression, rescued disease phenotypes including progressive weight loss and hepatocyte necrosis, and eliminated detectable off-target edits. Our findings establish fluorinated LNPs as an efficient and promising tool for mRNA delivery to enable precision base editing.

Introduction

Gene editing has revolutionized biomedical research by enabling durable corrections of disease-causing mutations [1–3]. Among pathogenic genetic variants, single base mutations account for nearly 50% of disease-associated mutations, positioning base editing as a pivotal therapeutic strategy [4,5]. Base editors (BEs), engineered through the fusion of Cas9 nickase (nCas9) with deaminases, achieve precise single-base conversions without inducing DNA double-stranded breaks (DSBs) or requiring donor DNA templates, thereby enhancing safety and efficacy compared to conventional CRISPR-Cas9 systems [4,6–8]. To broaden the therapeutic potential of base editing, extensive research efforts have been directed toward optimizing both the activity and precision of base editors [9–15]. We have engineered a series of highly efficient BEs, including hyA3A-BE4max, hyABE, eeBE4max, and eeA-BEmax, through the strategic incorporation of single- or double-stranded DNA binding domains into BE constructs [16–18]. Furthermore, through systematic protein engineering of deaminases, we have developed precision-enhanced BEs such as TdCBEs, ABE9, and haA3A-CBEs, which feature refined editing windows and significantly reduced off-target effects, representing a substantial advancement in the field of base editing technology [19–21].

Despite significant advancements in enhancing the activity and precision of base editors (BEs), their therapeutic efficacy *in vivo* is substantially influenced by delivery strategies. We and others have successfully employed dual adeno-associated virus (AAV) vectors for the efficient and precise correction of disease-associated mutations in murine models [21–23]. While AAV vectors offer high infection efficiency and versatile tissue tropism, several limitations hinder their clinical translation. These include restricted cargo capacity, potential immunogenicity, the risk of genomic integration, and sustained expression of editors/sgRNAs [24,25]. Lipid nanoparticles (LNPs) represent a

☆ This article is part of a special issue entitled: 'Nuclear Acid Therapeutics' published in Materials Today.

* Corresponding authors.
E-mail addresses: dlli@bio.ecnu.edu.cn (D. Li), yycheng@mail.ustc.edu.cn (Y. Cheng).

[1] These authors contributed equally to this work.

https://doi.org/10.1016/j.mattod.2026.103189
Received 16 May 2025; Received in revised form 12 January 2026; Accepted 14 January 2026

promising alternative for editor mRNA delivery, offering superior loading capacity that enables efficient co-delivery of various editor mRNAs and guide RNAs. [21,26–28]. By facilitating transient editor expression, LNPs help mitigate cumulative off-target effects and immune activation while minimizing bystander editing. The mRNA-based strategy also circumvents the insertional mutagenesis risks associated with DNA delivery. LNPs have been widely reported for delivering base editor mRNA to treat genetic diseases in mice and non-human primates [29–32]. However, a major limitation of conventional LNP systems is their inefficient endosomal escape, which often necessitates high mRNA and LNP doses to achieve therapeutic efficacy. This can lead to inflammatory responses and restrict the applicability of LNPs in base-editing therapies for genetic disorders[33–35].

To address this challenge, we developed a novel fluorinated LNP system. Fluorinated lipids self-assemble into stable nano-aggregates at low concentrations, enhancing nucleic acid encapsulation efficiency and complex stability. The fluorination strategy also optimizes key intracellular delivery processes, including cellular uptake, endosomal escape, and cargo release, thereby improving the efficacy and safety of polymeric nucleic acid carriers [36,37]. To further maximize the stabilizing effect of fluoroalkyl chains on mRNA encapsulation, we functionalized their terminal headgroups with catechol moieties. These groups strengthen mRNA binding through hydrogen-bond interactions, reinforcing the protective role of fluoroalkyl assembly, and have been shown to promote endosomal escape [38,39]. Our results demonstrate that incorporating fluoroalkyl chains markedly enhances the endosomal escape capability of conventional LNPs, leading to improved mRNA delivery efficiency both *in vitro* and *in vivo*. Using this optimized system, we delivered hyA3A-BE4max mRNA together with sgRNA to mouse hepatocytes, achieving up to 57.3% base editing efficiency at the Pcsk9 locus. In a mouse model of hereditary tyrosinemia type I [22], delivery of haA3A-CBE-VA via fluorinated LNPs specifically corrected the pathogenic Fah mutation by converting cytosine C_1 to thymine, while exhibiting negligible editing efficiency at adjacent cytosine sites C_{-2} and C_3. These findings underscore the high precision and therapeutic potential of this fluorinated LNP platform for base-editing therapies.

Results and discussion

Fluoroalkylated catechols (FCs) and lipidated catechols (LCs) were synthesized through esterification reactions between 3,4-dihydroxyhydrocinnamic acid and either fluoroalkyl alcohols or aliphatic alcohols (Fig. S1). The resulting compounds were characterized using ^{1}H NMR spectroscopy and ESI-MS, and designated as FC1, FC2, FC3, FC4, and LC1, LC2, LC3, LC4, based on the chain length and lipid pattern (Figs. 1a, S2, S3). Subsequently, both FCs and LCs were incorporated into a benchmark LNP formulation (Pfizer/BioNTech-derived) containing ALC0315, DSPC, cholesterol, and ALC0159 lipids. Previous studies have indicated that the introduction of polyphenolic or fluoroalkyl groups into delivery systems can markedly improve cargo encapsulation and facilitate endosomal escape. In such systems, the stoichiometric ratio between these functional ligands and ionizable lipids is known to critically influence overall delivery performance [38,40,41]. To systematically evaluate this effect, we prepared LNPs with varying molar ratios of FCs or LCs to the ionizable lipid ALC0315, specifically, 1:4 (FCn-1 or LCm-2), 1:3 (FCn-2 or LCm-2), 1:2 (FCn-3 or LCm-3), 1:1 (FCn-4 or LCm-

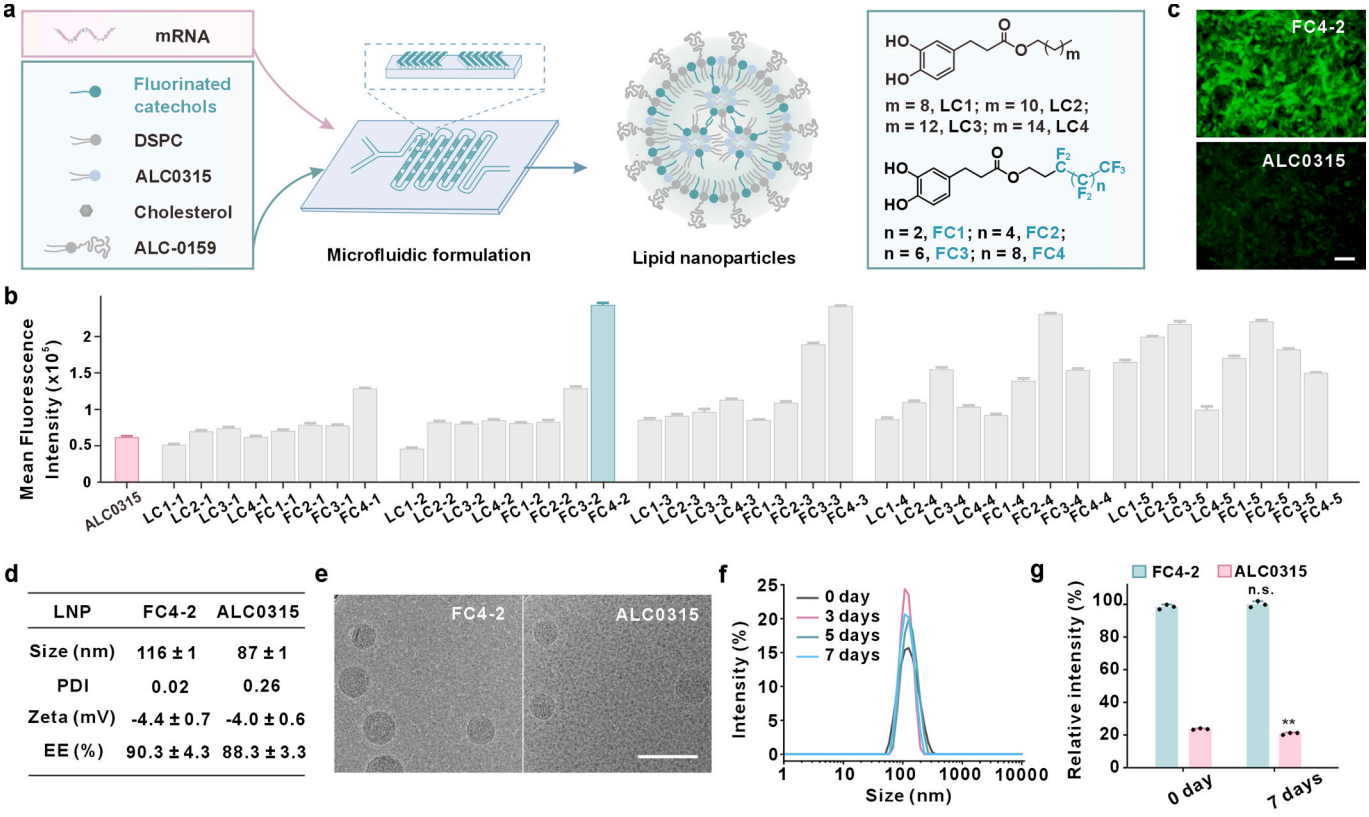

Fig. 1. Preparation and characterization of fluorinated LNPs for intracellular mRNA delivery. (a) Schematic representation of the preparation process for fluorinated LNPs. (b) Mean fluorescence intensity of 143B cells treated with LNPs incorporating FCs and LCs encapsulating EGFP mRNA. (c) Fluorescence microscopy images of 143B cells treated with ALC0315 and FC4-2 LNPs encapsulating EGFP mRNA. Scale bar: 100 μm. (d) Particle size, polydispersity index (PDI), zeta potential, and mRNA encapsulation efficiency (EE) of the LNPs. (e) Cryo-Transmission electron microscopy images of ALC0315 and FC4-2 LNPs. Scale bar: 100 nm. (f) Size distributions of FC4-2 LNPs after storage at 4 °C for 0–7 days. (g) Relative mean fluorescence intensity of 143B cells treated with LNPs stored at 4 °C for 0 day or 7 days, with the mean fluorescence intensity of cells treated with freshly prepared FC4-2 LNPs set as 100%, Statistical analysis was performed to assess the significance of differences between each type of LNP at day 0 and day 7 of storage.

4), and 2:1 (FCn-5 or LCm-5), and assessed their mRNA delivery efficiency. As shown in Fig. 1b, at lower molar ratios (e.g., 1:3 and 1:2), mRNA delivery efficiency increased with longer carbon or fluoroalkyl chains. In contrast, at higher molar ratios (such as 1:1 and 2:1), mRNA expression exhibited a non-monotonic trend, rising initially before declining as chain length increased. With respect to molar ratio effects, LNPs containing LCs or shorter fluoroalkyl chains (FC1 and FC2) showed progressively higher delivery efficiency as the proportion of FCs/LCs to the ionizable lipid increased. For longer-chain FCs (FC3 and FC4), however, delivery efficiency followed a bell-shaped relationship with molar ratio, peaking at intermediate ratios. Notably, FC4-2, which has a molar ratio of ALC0315: FC4: DSPC: cholesterol: ALC0159 = 46.3: 15.2: 42.7: 9.4: 1.6, achieved the highest intracellular mRNA delivery efficiency among all tested conditions, exceeding those of other FC- or LC-incorporated LNPs as well as the ALC0315 LNP (Fig. 1b). Besides 143B cells, the incorporation of FCs also significantly enhanced the mRNA delivery efficiency of ALC0315 LNPs in the mouse hepatocellular carcinoma cell line Hepa1-6 (Fig. S4). The incorporation of fluoroalkyl chains results in a slight increase in the size of the LNPs. FC4-2 LNPs displayed a uniform size distribution around 116 nm, possessed a nearly neutral electric charge, and achieved an mRNA loading efficiency of 90% (Fig. 1e, 1f). To further validate the versatility of our FCs incorporation strategy, we evaluated clinically approved ionizable lipid DLin-MC3-DMA- and SM102-based LNPs. Following the incorporation of FC4, we observed significant enhancements in protein expression in the cells treated with the modified LNPs (Figs. S5). These findings underscore the broad applicability of FCs incorporation in enhancing the mRNA delivery efficiency of LNPs. Given the instability of LNPs as a significant obstacle in practical applications, we investigated the mRNA delivery efficiency of FC4-2 LNPs after storage at 4 °C for varying durations. Notably, the FC4-2 LNPs exhibited remarkable stability, maintaining comparable mRNA delivery efficiency *in vitro* and *in vivo* even after 7 days of storage at 4 °C, without significant changes in the size (Fig. 1f, 1g, and S6, S7).

To determine whether the enhanced mRNA expression observed with FC4 incorporation is linked to improved cellular uptake efficiency,

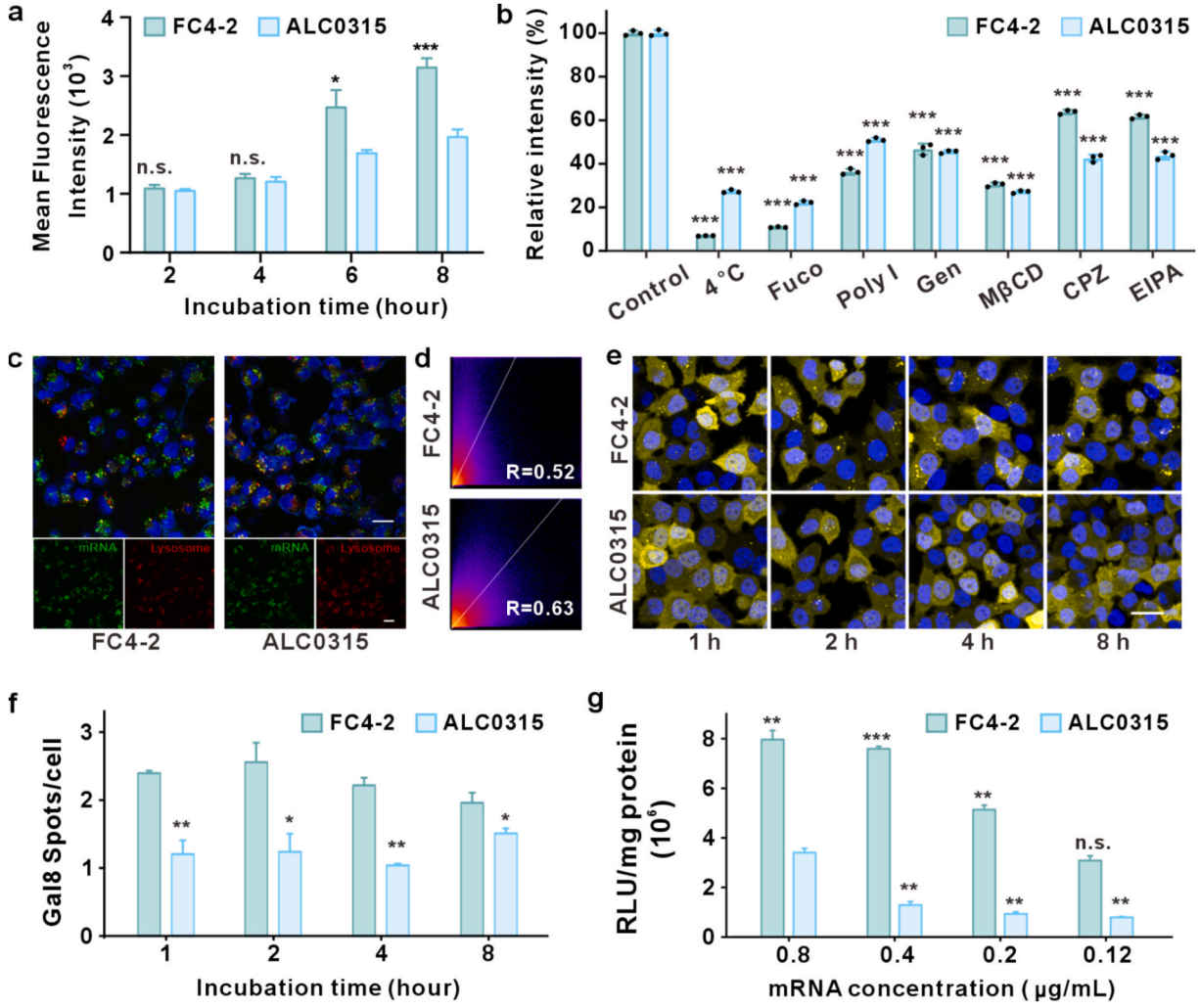

Fig. 2. Endocytosis and endosomal escape study of the LNPs. (a) Mean fluorescence intensity of 143B cells incubated with Cy5-labeled mRNA-encapsulated LNPs over various time points. (b) The relative fluorescence intensity of 143B cells treated with EGFP mRNA-containing LNPs for 24 h following pretreatment with inhibitors. The fluorescence intensity of cells treated with each LNP at 37 °C, without inhibitor pretreatment, was normalized to 100%. Statistically significant difference was observed between inhibitor-pretreated LNP groups and their corresponding controls at 37 °C. (c) Fluorescence images of 143B cells treated with Cy5-labeled mRNA-encapsulated LNPs for 6 h, with lysosomes and nuclei stained using LysoTracker Red and Hoechst 33342, respectively. (d) The intensity histogram displays the Pearson's correlation coefficient (R) for colocalization of Cy5-labeled mRNA and LysoTracker Red in (c). (e) Fluorescence images of HeLa-Gal8-YFP cells treated with luciferase mRNA-encapsulated LNPs at various time points. The nuclei were stained with Hoechst 33342. (f) Quantification of Gal8-YFP spots per cell. (g) Luciferase mRNA delivery efficiency of the LNPs in 143B cells at various mRNA concentrations. Statistical significance determined by a one-tailed Student's *t*-test, comparing each group to the ALC0315 group at the 0.8 μg/mL mRNA concentration. For (a) and (f), Statistical significance between the FC4-2 and ALC0315 LNP groups was evaluated using a one-tailed Student' s *t*-test, with ***P < 0.001, **P < 0.01, *P < 0.05, and $^{n.s.}$P ≥ 0.05. The scale bar is 20 μm in (c) and (e).

we encapsulated Cy5-labeled mRNA within FC4-2 and ALC0315 LNPs and monitored their cellular internalization at different time points (Fig. 2a, S8d). FC4-2 demonstrated comparable endocytosis efficiency to that of ALC0315 during the initial 2 h. However, by 6 and 8 h, the cellular uptake of FC4-2 surpassed that of ALC0315. Incubating at 4 °C, or pretreating the cells with inhibitors, such as fucoidan (Fuco), polyinosinic acid (Poly I), genistein (Gen), methyl-β-cyclodextrin (MβCD), chlorpromazine (CPZ), and ethyl-isopropylamiloride (EIPA), significantly inhibited cellular endocytosis of FC4-2 and ALC0315 LNP (Fig. 2b), indicating that the internalization process is energy-dependent and involves multiple pathways, such as scavenger receptor-mediated, caveolin-mediated, lipid raft-mediated, clathrin-mediated, and macropinocytosis-mediated mechanisms.

Endosomal escape is a critical step for efficient intracellular delivery of macromolecules. Previous studies have shown that fluoroalkane modifications can enhance the endosomal escape capabilities of delivery systems [42]. To evaluate the impact of FC4 incorporation on the endosomal escape efficiency of LNPs, we employed confocal microscopy to assess the colocalization of LNPs with *endo*-lysosomes. At 6 h post-treatment, while Cy5-labeled ALC0315 LNPs predominantly remained colocalized with lysosomes, exhibiting a Pearson's colocalization coefficient more than 0.63, a significant higher proportion of Cy5-labeled FC4-2 LNPs had escaped from endosomes in both 143B and Hepa 1–6 cells (Fig. 2c, 2d, S8e). Additionally, we utilized the HeLa-Gal8-YFP cell line, which stably expresses a fusion protein consisting of Galectin 8 (Gal8) and yellow fluorescent protein (YFP) to study the endosomal escape efficiency of the LNPs. Gal8, a β-galactoside-binding lectin, is typically found in the cytoplasm but rapidly translocates to damaged endosomes following membrane rupture due to its high affinity for galactosides in the inner leaflet of the endosomal membrane. This translocation results in visible fluorescent puncta, facilitating the quantification and examination of endosomal rupture [43]. As shown in Fig. 2e–f, cells treated with FC4-2 LNPs exhibited prominent yellow fluorescence spots at 1 h post-treatment, reaching peak intensity at 2 h, which was much more efficient than that of ALC0315 LNP. Due to its efficient endosomal escape capability, FC4-2 effectively reduced the required mRNA dose for delivery, achieving protein expression levels comparable to those of ALC0315 at less than one-sixth of the mRNA dose (Fig. 2g).

To further investigate the contribution of the catechol moiety in FC4 to enhancing LNP-mediated mRNA delivery, we synthesized a control lipid (FC4Q) by chemically quenching the catechol functionality (Fig. S8a). FC4Q-2 LNPs were prepared by substituting FC4 with FC4Q in the FC4-2 formulation, and their mRNA delivery performance was evaluated. Notably, FC4Q-2 LNPs exhibited significantly reduced delivery efficiency compared to FC4-2 LNPs (Fig. S8b), underscoring the critical role of the catechol group for optimal LNP function. Physicochemical characterization showed that FC4Q-2 LNPs had a larger hydrodynamic diameter and lower mRNA encapsulation efficiency than FC4-2 LNPs (Fig. S8c), suggesting that catechol groups facilitate mRNA binding and encapsulation. Cellular assays revealed that both FC4Q-2 and FC4-2 mediated comparable levels of cellular uptake (Fig. S8d) and endosomal escape (Fig. S8e), with both outperforming the commercial benchmark ALC0315 LNP. These findings indicate that the fluorinated alkyl chains are primarily responsible for promoting membrane interaction and endosomal escape.

To evaluate the *in vivo* mRNA delivery efficacy of the fluorinated LNPs, we performed comparative analyses of luciferase expression after intravenous administration of luciferase mRNA-loaded LNPs. Whole-body bioluminescence imaging revealed significantly enhanced mRNA delivery efficiency upon FC4 lipid incorporation (Fig. 3a, 3b), with FC4-2 LNPs showing the highest delivery performance among the tested formulations. The LNPs largely retained the original tissue tropism profile, with predominant hepatic accumulation (Fig. 3c). Quantitative

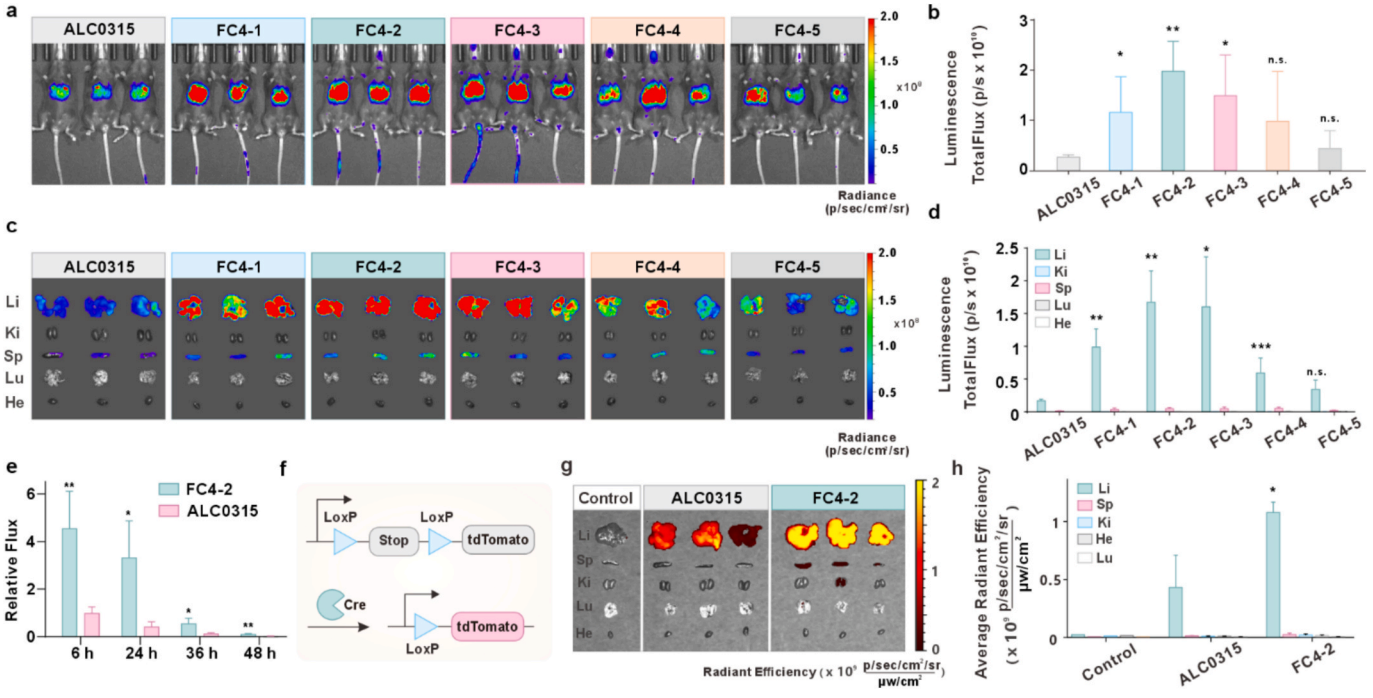

Fig. 3. *In vivo* mRNA delivery efficiency of LNPs via intravenous injection. (a) Bioluminescence images of mice 6 h after intravenous injection with Luci mRNA-bearing LNPs. (b) Total luminescence intensity of the mice shown in (a). (c) Bioluminescence images of the liver (Li), spleen (Sp), kidney (Ki), heart (He), and lung (Lu) from mice 6 h after intravenous injection with Luci mRNA-bearing LNPs. (d) Total luminescence intensity of the organs shown in (c). (e) Relative total luminescence intensity of the mice 6 h to 48 h after intravenous injection with Luci mRNA-bearing LNPs, and the total luminescence intensity of the mice treated with ALC0315 LNP for 6 h was set as 1. (f) Diagram of Cre recombinase-mediated tdTomato protein expression in Ai14 mice. (g) Fluorescence images of the liver (Li), spleen (Sp), kidney (Ki), heart (He), and lung (Lu) from Ai14 mice 48 h after intravenous injection with Cre mRNA-bearing LNPs. (h) tdTomato fluorescence intensity of the organs shown in (g). n = 3. Statistically significant differences were assessed between the FC4-2 and the ALC0315 LNP groups using a one-tailed Student's *t*-test.

analysis indicated that FC4-2 LNPs yielded at about 5-fold higher hepatic luciferase expression than ALC0315-based LNPs (Fig. 3d). Expression kinetics assessment showed that ALC0315 LNPs exhibited a progressive decline in luciferase activity, with notable reduction at 24 h and minimal levels by 36 h (Fig. 3e, and S9). In contrast, FC4-2 LNPs displayed delayed expression kinetics. At 24 h, FC4-2 maintained protein expression levels exceeding 2-fold the peak levels observed with ALC0315 LNPs at 6 h. By 36 h, although FC4-2 expression had declined, it remained comparable to ALC0315 LNPs at 24 h. At 48 h, FC4-2 expression decreased to levels similar to those of ALC0315 LNPs at 36 h. Collectively, these results demonstrate that FC4-2 LNPs significantly extend the duration of *in vivo* mRNA expression, highlighting their superior ability to prolong therapeutic protein production. To further confirm functional mRNA delivery, we used Ai14 reporter mice, which harbor a LoxP-flanked tdTomato reporter cassette (Fig. 3f). Systemic administration of Cre mRNA-loaded FC4-2 LNPs induced efficient excision of the stop cassette, as evidenced by strong tdTomato fluorescence specifically in liver tissues. Comparative analysis showed that the recombination efficiency in mice treated with FC4-2 LNPs was approximately one-fold higher than that in the ALC0315 LNP group (Fig. 3g, 3h), confirming the enhanced functional mRNA delivery capacity of the FC4-optimized formulation.

We next investigated FC4-2 LNPs for therapeutic base editing by targeting PCSK9, a hepatic regulator of LDL receptor metabolism. We employed the hyA3A-BE4max base editor [16], which we developed with high activity and a broad editing window, to efficiently inactivate Pcsk9 by introducing a premature stop codon at the W159 codon (Fig. 4a, 4b). FC4-2 LNPs co-encapsulating hyA3A-BE4max mRNA and sgRNA (1:1 w/w ratio) were administered intravenously (1 mg/kg) to C57BL/6J mice. High-throughput sequencing revealed efficient C-to-T conversion at target sites C7 (57.3% ± 6.6%) and C8 (50.8% ± 7.0%) one-month post-injection (Fig. 4c). This durable editing correlated with 66% reduction in serum PCSK9 levels, subsequently decreasing LDL cholesterol, total cholesterol, and triglycerides versus non-treated mice (Fig. 4d–g). ELISA analysis confirmed treatment safety with no evidence of hepatic inflammation or injury (Fig. 4h–m, Fig. S10). Histopathological examination via H&E staining of tissue sections from major organs (heart, liver, spleen, lung, and kidney) revealed no apparent pathological alterations or signs of tissue damage in any of the organs from the FC4-2 LNP-treated group compared to the PBS-treated controls at this dosage (Fig. S11).

We further investigated the capability of FC4-2 LNP to deliver haA3A-CBE-VA, which we engineered to exhibit minimal off-target activity and a narrowed editing window for precise correction of a point mutation in a mouse model of HT1 (Fig. 5a) [22]. The HT1 mouse harbors an A-to-G substitution at the start codon of Fah gene ($Fah^{NS/NS}$), resulting in the loss of Fah expression and consequent severe liver damage (Fig. 5b). The mRNA encoding haA3A-CBE-VA and the sgRNA

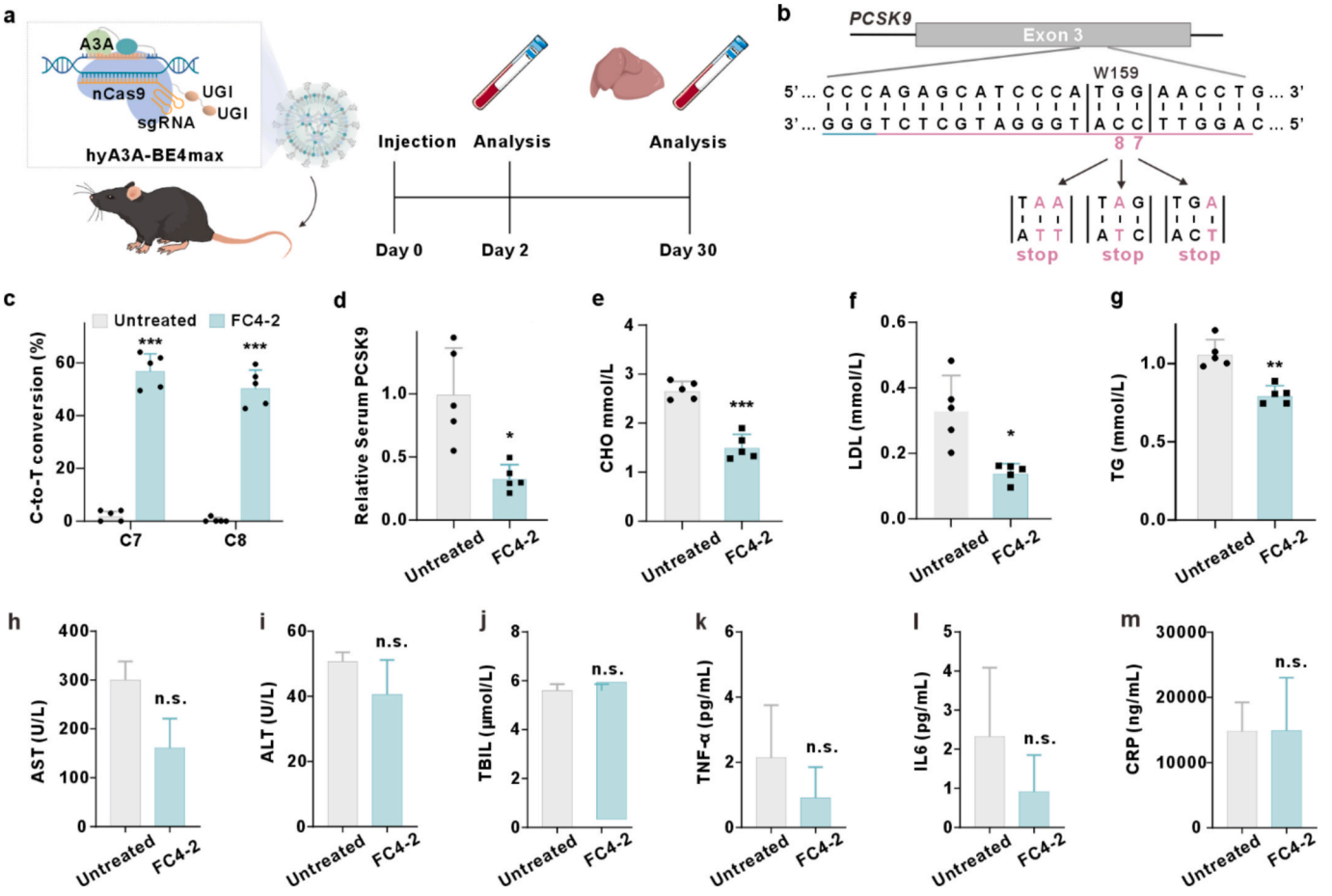

Fig. 4. *In vivo* delivery of hyA3A-BE4max mRNA and sgRNA for PCSK9 editing. (a) Structure of hyA3A-BE4max and the timeline of the *in vivo* test for single-base editor delivery. (b) Schematic representation of single-base editing at the W159 target site in the PCSK9 gene using hyA3A-BE4max, converting W159 to a stop codon to prevent PCSK9 protein expression. (c) C-to-T editing frequencies in mice a month after treatment with FC4-2 LNPs encapsulating hyA3A-BE4max mRNA and sgRNA targeted to PCSK9. (d) Relative serum concentrations of PCSK9. Concentrations of serum cholesterol (CHO) (e), low-density lipoprotein cholesterol (LDL) (f), and triglycerides (TG) (g) a-month post *in vivo* gene editing, n = 5. Concentrations of aspartate aminotransferase (AST) (h), alanine aminotransferase (ALT) (i), total bilirubin (TBIL) (j), and inflammatory cytokines TNF-α (k), IL-6 (l), and C-reactive protein (CRP) (m) in the blood 48 h after LNP injection, n = 3. Statistically significant differences were assessed between the FC4-2 LNP and the untreated group using a one-tailed Student's *t*-test.

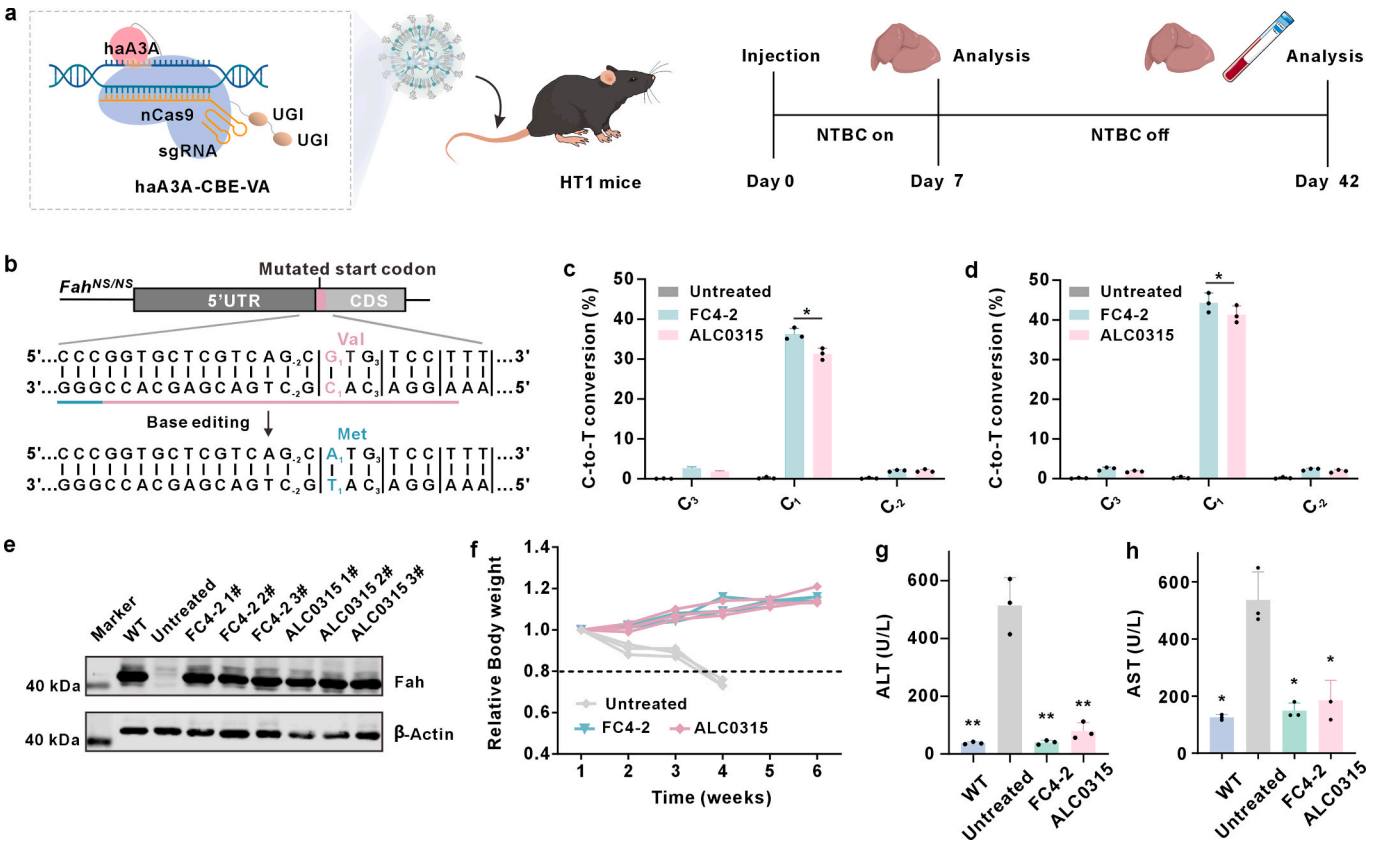

Fig. 5. *In vivo* delivery of haA3A-CBE-VA mRNA and sgRNA for HT1 therapy. (a) Structure of haA3A-CBE-VA and the timeline of the treatment of HT1. (b) Diagram of a sgRNA designed to target the mutated start codon of $Fah^{NS/NS}$ allele. PAM and protospacer are indicated by a green line, and a pink line, respectively. Editing efficiency of the targeted cytosines (c) 1 week or (d) 6 weeks after LNP administration. (e) Western blot analysis of Fah protein expression in mouse liver tissue 6 weeks after LNP administration. (f) Changes in mice weight following NTBC withdrawal, normalized to baseline from week 1. Serum (g) ALT and (h) AST levels in peripheral blood from mice 6 weeks after LNP administration. Statistically significant differences were evaluated between each group and the untreated HT1 group using a one-tailed Student's *t*-test.

targeting the Fah start codon were co-encapsulated into both FC4-2 LNPs and ALC0315 LNPs. Six-week-old HT1 mice were intravenously administered the LNPs. One week after treatment, FC4-2 LNPs mediated an average C-to-T editing efficiency of 36.2% at the target site (C_1) in the liver, which was significantly higher than that achieved with ALC0315 LNPs (31.3%) (Fig. 5c). Following a 5-week withdrawal of NTBC (2-(2-nitro-4-trifluoromethylbenzoyl)-1,3-cyclohexanedione; a life-saving drug for HT1), the corrected allele frequency further increased to 44.3% in the FC4-2 group, also significantly surpassing the ALC0315 group (Fig. 5d). Both LNP formulations exhibited minimal editing at off-target sites (C_3 and C_{-2}), demonstrating high specificity. This efficient editing restored FAH protein expression (Fig. 5e) and prevented weight loss and liver injury after NTBC withdrawal (Fig. 5f–h, and S12).

However, although FC4-2 LNPs led to higher editing efficiency, the corresponding advantages in body weight recovery and serum liver function biomarkers were not statistically significant compared to the ALC0315 group. This observation can be explained by two main reasons. First, the FC4-2 formulation was initially optimized using luciferase mRNA, which may not represent the optimal formulation for base-editor delivery, thus limiting its comparative advantage over ALC0315 LNPs. Second, in monogenic diseases such as hereditary tyrosinemia, even a low level of genetic correction can elicit a therapeutic response due to the strong selective growth advantage of corrected hepatocytes. Once a threshold level of Fah-positive cells is achieved, liver function is sufficiently restored to support normal physiological metrics, such as survival, weight gain, and serum biomarkers, resulting in a plateau effect where additional editing confers diminishing phenotypic returns. In our study, both ALC0315 and FC4-2 treatments restored liver function to wild-type levels, with FC4-2 showing a non-significant trend toward improvement, suggesting that the functional saturation threshold had been reached. It should be noted that higher editing efficiency may still offer benefits such as faster recovery, greater long-term stability, and enhanced resilience to subsequent hepatic stress. These results also highlight the importance of tailoring LNP formulation to specific cargo molecules and disease models in future applications.

Conclusion

In conclusion, this study introduces an innovative strategy to augment the endosomal escape efficiency and stability of lipid nanoparticles through the incorporation of fluorolipids. This advancement significantly enhances their ability to efficiently deliver mRNA both *in vitro* and *in vivo*. Notably, the engineered FC4-2 LNPs exhibited exceptional performance in delivering a range of mRNA cargoes, encompassing EGFP, luciferase, Cre recombinase, and single-base editors, into liver cells. The successful delivery of hyA3A-BE4max along with its corresponding sgRNA facilitated efficient editing of the PCSK9 gene, leading to a substantial reduction in blood cholesterol and triglyceride levels, which holds promise for the treatment of hypercholesterolemia. Additionally, FC4-2 LNPs demonstrated robust delivery of the highly accurate single-base editor haA3A-CBE-VA and its targeting sgRNA into the livers of $Fah^{NS/NS}$ HT1 model mice. This resulted in precise C-to-T conversion at the mutated site of the Fah gene, thereby restoring Fah protein expression and effectively alleviating weight loss and liver damage in these animals. Collectively, our findings underscore the

tremendous potential of FC4-2 LNPs as a therapeutic platform for the delivery of single-base editor mRNA, offering a promising approach for the treatment of genetic diseases characterized by single-base mutations.

Materials and methods

Materials. 3-(3,4-Dihydroxyphenyl) propionic acid (98%), 1H,1H,2H,2H-Perfluorohexan-1-ol (97%), 1H,1H,2H,2H-Heptadecafluoro-1-decanol (97%), and 1H,1H,2H,2H-Perfluoro-1-dodecanol (97%) were purchased from Energy Chemical (Shanghai, China). 1H,1H,2H,2H-Perfluorooctan-1-ol (97%), 1-Decanol (98%), 1-Dodecanol (99%), 1-Tetradecanol (98%), 1-Hexadecanol (98%), 4-dimethylaminopyridine (DMAP, 99%), Trifluoroacetic acid, and N,N'-diisopropylcarbodiimide (DIPC, 99%) were from J&K Scientific (Shanghai, China). Phosphorus trichloride (99%), Acetone (anhydrous, 99%), Ethyl acetate (EtOAc, reagent grade), Dichloromethane (DCM, reagent grade), and Petroleum ether (PE, reagent grade) were purchased from Kelong Chemical (Chengdu, China). ALC0315, DLin-MC3-DMA, SM102, DMG-PEG 2000, DSPC, and ALC0159 were purchased from Sinopeg (Xiamen, China). Cholesterol was purchased from Macklin (Shanghai, China). Cy5-labelled mRNA ($mRNA_{Cy5}$) was purchased from ApexBio (Houston, USA). Mouse PCSK9 ELISA Kit (ab215538) and Ribogreen were purchased from Abcam (Boston, USA) and Shinegene (Shanghai, China), respectively. FastPure Cell/Tissue DNA isolation mini kit and 2x Phanta max master mix were purchased from Vazyme (Nanjing, China). IVISbrite D-luciferin potassium salt bioluminescent substrate was purchased from Revvity (Waltham, USA). Hoechst was purchased from Beyotime (Shanghai, China). sgRNAs bearing phosphorothioate and 2′-O-methyl modifications at positions1-3 at both the 5′ and 3′ termini were ordered from GenScript Probio (Nanjing, China). Anti-FAH antibody was bought from AbboMax (San Jose, USA). Anti-β-actin antibody was purchased from Sigma (St. Louis, USA). The PCR primers were purchased from Sangon Biotech (Shanghai, China). The sequences of sgRNAs and the primers were listed in Table S1.

Synthesis and characterization of FCs and LCs

Synthesis of Acetonide-Protected 3,4-Dihydroxyhydrocinnamic Acid (1): 3,4-Dihydroxyhydrocinnamic acid (5.00 g, 27.44 mmol) was dissolved in 60 mL of anhydrous acetone. After chilling in an ice bath for 10 min, phosphorus trichloride (2.00 mL, 22.98 mmol) was gradually added via syringe. The mixture was allowed to react at room temperature for 6 h, followed by removal of acetone through rotary evaporation under reduced pressure. The residue was then redissolved in 300 mL of ethyl acetate and sequentially washed with deionized water and saturated brine. The organic layer was collected, concentrated, and the resulting crude product was purified by flash column chromatography (silica gel, EtOAc/PE (v/v = 1/2) as eluent), yielding a white powder (2.73 mg, 44.7%).

Synthesis of FCs and LCs: The FCs and LCs were synthesized using a similar method: 660 mg DMAP, 4.05 mmol R-CH_2CH_2-OH, and 600 mg Acetonide-protected 3,4-dihydroxyhydrocinnamic acid were mixed in 5 mL DCM. After stirring 10 min in an ice bath, 4.50 mmol DIPC was carefully introduced. The reaction mixture was stirred at room temperature for 24 h, and the solvent was then evaporated under reduced pressure to obtain a crude product. Purification by column chromatography (silica gel, DCM/PE (v/v = 1/5) as eluent) resulted in a series of yellow oily or solid products (Yield: 71%-85%). Subsequently, 600 mg of the fluorinated/lipidated catechol was dissolved in 6 mL of a DCM and Trifluoroacetic acid mixed solvent (v/v = 4: 2). After 6 h of stirring, the solvent was removed under high vacuum, and the crude product was washed repeatedly with hexane and dried, yielding a white powder sample (Yield: 85%-91%).

Characterization of FCs and LCs: All ^1H nuclear magnetic resonance (NMR) spectra were acquired in $CDCl_3$ (Aldrich, 99.8% D) using a Bruker AV III HD 400 MHz spectrometer at room temperature.

RNA Synthesis and Purification. mRNAs encoding EGFP, Luciferase, CRE, hyA3A-BE4max, and haA3A-CBE-VA containing 5′-cap and poly(A) tail modifications along with N1-methyl pseudouridine (N1-Me-pseudo-U) were transcribed from linearized plasmid DNA templates and a high-yield T7 *in vitro* transcription kit containing N1-Me-pUTP (Hzmes Biotech, Catalog No. HBP001505). Subsequently, the mRNAs were isolated by precipitation with ammonium acetate, following the manufacturer's protocol. The concentrations of the transcripts were determined by measuring absorbance at 260 nm using a Nanodrop spectrophotometer.

Preparation and Characterization of LNPs. For the ALC0315 LNP, ALC0315, cholesterol, DSPC, and ALC0159 were combined at a molar ratio of 46.3: 42.7: 9.4: 1.6 in ethanol. RNAs were mixed in acetate buffer (50 mM, pH 4.5). The LNPs were formed by mixing the lipid and RNA solutions with a 1:3 ethanol-to-aqueous flow rate ratio in microfluidic device (AITESEN, China). The N/P ratio was fixed at 4.5. The resultant mixture was diluted with an equal volume of PBS (pH 7.4), followed by buffer exchange into PBS using an Amicon® Ultra centrifugal filter (10 kDa molecular weight cutoff). FC- or LC-incorporated LNPs were prepared by varying the molar ratio of FCs or LCs to the ionizable lipid ALC0315, specifically, 1:4, 1:3, 1:2, 1:1, and 2:1, while keeping the molar ratios of the other four lipid components (DSPC, cholesterol, and ALC0159) constant. The resulting formulations were designated as FCn-1/LCm-1 (1:4), FCn-2/LCm-2 (1:3), FCn-3/LCm-3 (1:2), FCn-4/LCm-4 (1:1), and FCn-5/LCm-5 (2:1), respectively.

For the SM102 LNP, the molar ratio of SM102: DSPC: cholesterol: PEG2000-DMG was 50: 10: 38.5: 1.5. For the FC4-SM102 LNP, the molar ratio of SM102: FC4: DSPC: cholesterol: PEG2000-DMG was 50: 25: 10: 38.5: 1.5.

For the MC3 LNP, the molar ratio of MC3: DSPC: cholesterol: PEG2000-DMG was 50: 10: 38.5: 1.5. For the FC4-MC3 LNP, the molar ratio of MC3: FC4: DSPC: cholesterol: PEG2000-DMG was 50: 25: 10: 38.5: 1.5.

The hydrodynamic diameter, polydispersity index (PDI), and zeta potential of the prepared LNPs were characterized using Zetasizer (Malvern, UK). The morphologies of the LNPs were observed using cryogenic transmission electron microscopy (Thermo scientific, the Czech Republic). The mRNA encapsulation efficiencies were tested by a Ribogreen assay.[44] Specifically, the LNP solution was lysed with Triton-X-100, enabling the quantification of total RNA content through RiboGreen detection. An equal volume of untreated LNP solution (lacking Triton-X-100) was directly assayed with RiboGreen to measure the amount of unencapsulated RNA. The RNA encapsulation ratio was determined by calculating the difference in RNA quantity between the lysed and untreated samples, and dividing this difference by the total RNA quantity in the lysed solution.

Cell Cultures. Human osteosarcoma 143B cells, human cervical carcinoma HeLa cells, HeLa-Gal8-YFP, and mouse hepatoma Hepa 1–6 cells were cultured in Dulbecco's Modified Eagle Medium (DMEM, GIBCO) supplemented with penicillin sulphate (100 units/mL), streptomycin (100 μg/mL), and 10% fetal bovine serum (FBS, GIBCO) at 37 °C with 5% CO_2.

***In vitro* mRNA Delivery.** 143B cells were seeded in 48-well plates and incubated overnight until 80%-90% confluence, then treated with EGFP or luci mRNA-encapsulated LNPs for 24 h. For EGFP mRNA delivery, the protein expression was observed via fluorescence microscope (Olympus, Japan), and quantitively analyzed by flow cytometer (Beckman Coulter, USA). For luci mRNA delivery, the luciferase protein expression was assayed following the manufacturer's protocols provided by Promega. The protein concentration in each well was quantified using a BCA protein assay kit from Beyotime. The luciferase activities were then normalized to the relative luciferase light units per milligram of protein (RLU/mg protein).

To study cellular uptake efficiency of the LNPs, 143B cells were cultured in 48-well plates overnight until they reach 80%-90%

confluence. The cells were then treated with $mRNA_{Cy5}$ encapsulated LNP for 1, 2, 4, or 8 h. The cell internalization of the LNPs was quantitatively analyzed by flow cytometry (Beckman Coulter, USA).

To investigate the endosomal disruption efficiency of the LNPs, HeLa-Gal8-YFP cells were seeded in 48-well plates and incubated overnight until they reached 80%-90% confluence. The cells were then treated with LNPs encapsulating luciferase mRNA for 1, 2, 4, or 8 h. The cells were stained with Hoechst, and the recruitment of Gal8-YFP (indicating endosomal disruption) was visualized using a laser scanning confocal microscope (Leica, Germany). The average number and area of Gal8-YFP puncta in the treated cells were quantitatively analyzed using ImageJ, with 200 cells counted in each experimental group.

Intracellular Base-editing study. Hepa 1–6 cells were seeded in 24-well plates and incubated overnight until they reached 30%-40% confluence. The cells were then treated with FC4-2 LNP encapsulated with hyA3A-BE4max mRNA and sgRNA targeting PCSK9 at a 1:1 M ratio, and incubated for 72 h. After that, genomic DNA of the treated cells was extracted, and PCSK9 gene fragment was amplified using PCR. The base editing efficiency at the target site was analyzed using Sanger sequencing.

Additionally, a stable cell line, $Fah^{NS/NS}$ HEK293, was generated via lentiviral transfection with a target sequence that contains $Fah^{NS/NS}$ allele [22]. The $Fah^{NS/NS}$ HEK293 cells were cultured in 24-well plates overnight until they reached 30%-40% confluence, and then treated with FC4-2 LNP encapsulated with haA3A-CBE-VA mRNA, UGI mRNA, and sgRNA in a weight ratio of 4:1:4. After 72-h incubation, genomic DNA was extracted, and the target *Fah* gene fragment was amplified by PCR. The efficiency of the C•G-to-T•A transition at the target site was determined using Sanger sequencing.

***In vivo* mRNA Delivery.** The wild-type C57BL/6J mice were purchased from Shanghai Laboratory Animal Center. All animal experiments were conducted in strict compliance with the NIH guidelines and approved by the ethics committee of East China Normal University.

For luciferase mRNA delivery, mice were administered with luciferase mRNA-encapsulated LNPs at a dose of 0.25 mg/kg via tail vein injection. 6 hours later, the mice were intraperitoneally injected with 200 μL of d-luciferin (15 mg/mL) and incubated for 8 min. Subsequently, the mice were anesthetized, and luciferase expression was observed using the IVIS spectrum imaging system (PerkinElmer, USA). Following imaging, the mice were euthanized, and their organs were extracted for further observation via the IVIS spectrum.

For Cre mRNA delivery, Ai14 mice were randomly divided into three groups (untreated, ALC0315 and FC4-2 LNPs), with three mice in each group. The mice were treated with Cre mRNA-encapsulated LNPs at a dose of 0.05 mg/kg. 48 h later, the mice were euthanized via cervical dislocation, and their organs were extracted. The expression of tdTomato in the organs was subsequently observed using the IVIS imaging system (PerkinElmer, USA).

Base-editing for PCSK9 Disruption. Wild-type C57BL/6J mice were randomly divided into two groups (untreated and FC4-2). The FC4-2 group was administered FC4-2 LNP encapsulating hyA3A-BE4max mRNA and sgRNA targeting PCSK9 at a 1:1 weight ratio. The mice were incubated for a month post-injection. Following this period, the treated mice were euthanized immediately after blood collection, and liver tissue was obtained. Serum was separated from the collected blood by centrifugation, and serum ALT, AST, and TBIL levels were measured by Servicebio. The serum PCSK9 level was tested using a Mouse PCSK9 ELISA Kit (Abcam, ab215538) according to the manufacturer's protocol.

Base-editing for the treatment of HT1. $Fah^{NS/NS}$ mice were obtained via CRISPR-based gene editing as previously described [22]. The drinking water for $Fah^{NS/NS}$ mice was supplemented with 10 mg/L NTBC for protection against liver damage. For $Fah^{NS/NS}$ mice treatment experiments, the haA3A-CBE-VA mRNA, sgRNA, and UGI mRNA were co-encapsulated in FC4-2 or ALC0315 LNPs at a mass ratio of 4:4:1. 6-week-old $Fah^{NS/NS}$ mice were administered with the LNPs via tail vein injection (3 mg/kg). One-week post-injection, biopsy was performed to collect liver tissues, and then NTBC was withdrawn to allow corrected hepatocytes to proliferate. Five weeks after NTBC withdrawal, treated mice were euthanized immediately following the blood collection, and liver tissue were obtained. Untreated control mice were euthanized when they lost over 20% body weight. ALT, TBIL and AST levels in serum were measured by Servicebio.

HTS and data analysis. Genomic DNA was extracted from mouse liver tissues using the TIANamp Genomic Kit (Tiangen Biotech, DP304-03), and then, the purified DNA was used as templates for amplifying genomic regions of interest. The primer sequences were listed in Table S1. HTS library was produced by a second round of PCR using above products and primers containing unique barcode sequences, and then sequenced on an Illumina HiSeq platform. The BE-Analyzer was used to analyze the HTS data and output the base editing rates [45].

CRediT authorship contribution statement

Jia Lv: Writing – review & editing, Writing – original draft, Visualization, Methodology, Investigation, Funding acquisition, Formal analysis, Data curation. **Lei Yang:** Writing – review & editing, Writing – original draft, Visualization, Methodology, Investigation, Formal analysis, Data curation. **Xi Chen:** Writing – original draft, Methodology, Investigation, Data curation. **Jin Zhang:** Investigation, Data curation. **Zhan Li:** Investigation. **Jianan Duan:** Investigation. **Tianai Zhang:** Investigation. **Yiwen Li:** Methodology. **Dali Li:** Writing – review & editing, Supervision, Resources, Project administration, Conceptualization. **Yiyun Cheng:** Writing – review & editing, Supervision, Resources, Project administration, Conceptualization.

Declaration of competing interest

The authors declare that they have no known competing financial interests or personal relationships that could have appeared to influence the work reported in this paper.

Acknowledgments

This work was supported by the National Natural Science Foundation of China (U25A20258 and 52373134, 32025023), and the Instruments Sharing Platform of School of Life Sciences and Multifunctional Platform for Innovation (004 and 011) at East China Normal University.

Appendix A. Supplementary material

Supplementary data to this article can be found online at https://doi.org/10.1016/j.mattod.2026.103189.

Data availability

Data will be made available on request.

References

[1] M. Jinek, K. Chylinski, I. Fonfara, M. Hauer, J.A. Doudna, E. Charpentier, Science. 337 (2012) 816–821.
[2] A. Raguram, S. Banskota, D.R. Liu, Cell 185 (2022) 2806–2827.
[3] Y. Lyu, C. Yang, X. Lyu, K. Pu, Small 17 (2021) 202005222.
[4] N.M. Gaudelli, A.C. Komor, H.A. Rees, M.S. Packer, A.H. Badran, D.I. Bryson, D. R. Liu, Nature 551 (2017) 24644.
[5] Y. Wang, J.A. Doudna, Science. 379 (2023) 8643.
[6] H.A. Rees, D.R. Liu, Nat. Rev. Genet. 19 (2018) 770–788.
[7] A.C. Komor, Y.B. Kim, M.S. Packer, J.A. Zuris, D.R. Liu, Nature 533 (2016) 420–424.
[8] K. Nishida, T. Arazoe, N. Yachie, S. Banno, M. Kakimoto, M. Tabata, M. Mochizuki, A. Miyabe, M. Araki, K.Y. Hara, Z. Shimatani, A. Kondo, Science 353 (2016) 8729.
[9] M. Pacesa, O. Pelea, M. Jinek, Cell 187 (2024) 1076–1100.

[10] M.F. Richter, K.T. Zhao, E. Eton, A. Lapinaite, G.A. Newby, B.W. Thuronyi, C. Wilson, L.W. Koblan, J. Zeng, D.E. Bauer, J.A. Doudna, D.R. Liu, Nat. Biotechnol. 38 (2020) 883–891.
[11] C. Li, Y. Zong, Y. Wang, S. Jin, D. Zhang, Q. Song, R. Zhang, C. Gao, Genome Biol. 19 (2018) 59.
[12] S. Suh, E.H. Choi, H. Leinonen, A.T. Foik, G.A. Newby, W.-H. Yeh, Z. Dong, P. D. Kiser, D.C. Lyon, D.R. Liu, K. Palczewski, Nat. Biomed. Eng. 5 (2020) 169–178.
[13] S. Li, B. Yuan, J. Cao, J. Chen, J. Chen, J. Qiu, X.-M. Zhao, X. Wang, Z. Qiu, T.-L. Cheng, Nat. Commun. 11 (2020) 5827.
[14] N.M. Gaudelli, D.K. Lam, H.A. Rees, N.M. Solá-Esteves, L.A. Barrera, D.A. Born, A. Edwards, J.M. Gehrke, S.-J. Lee, A.J. Liquori, R. Murray, M.S. Packer, C. Rinaldi, I.M. Slaymaker, J. Yen, L.E. Young, G. Ciaramella, Nat. Biotechnol. 38 (2020) 892–900.
[15] K. Xu, H. Feng, H. Zhang, C. He, H. Kang, T. Yuan, L. Shi, C. Zhou, G. Hua, Y. Cao, Z. Zuo, E. Zuo, Nat. Biomed. Eng. 9 (2025) 93–108.
[16] X. Zhang, L. Chen, B. Zhu, L. Wang, C. Chen, M. Hong, Y. Huang, H. Li, H. Han, B. Cai, W. Yu, S. Yin, L. Yang, Z. Yang, M. Liu, Y. Zhang, Z. Mao, Y. Wu, M. Liu, D. Li, Nat. Cell Biol. 22 (2020) 740–750.
[17] N. Xue, X. Liu, D. Zhang, Y. Wu, Y. Zhong, J. Wang, W. Fan, H. Jiang, B. Zhu, X. Ge, R.V.L. Gonzalez, L. Chen, S. Zhang, P. She, Z. Zhong, J. Sun, X. Chen, L. Wang, Z. Gu, P. Zhu, M. Liu, D. Li, T.P. Zhong, X. Zhang, Nat. Commun. 14 (2023) 1224.
[18] S. Yin, M. Zhang, Y. Liu, X. Sun, Y. Guan, X. Chen, L. Yang, Y. Huo, J. Yang, X. Zhang, H. Han, J. Zhang, M.-M. Xiao, M. Liu, J. Hu, L. Wang, D. Li, Mol. Ther. 31 (2023) 744–759.
[19] L. Chen, B. Zhu, G. Ru, H. Meng, Y. Yan, M. Hong, D. Zhang, C. Luan, S. Zhang, H. Wu, H. Gao, S. Bai, C. Li, R. Ding, N. Xue, Z. Lei, Y. Chen, Y. Guan, S. Siwko, Y. Cheng, G. Song, L. Wang, C. Yi, M. Liu, D. Li, Nat. Biotechnol. 41 (2023) 663–672.
[20] L. Chen, S. Zhang, N. Xue, M. Hong, X. Zhang, D. Zhang, J. Yang, S. Bai, Y. Huang, H. Meng, H. Wu, C. Luan, B. Zhu, G. Ru, H. Gao, L. Zhong, M. Liu, M. Liu, Y. Cheng, C. Yi, L. Wang, Y. Zhao, G. Song, D. Li, Nat. Chem. Biol. 19 (2023) 101–110.
[21] L. Yang, Y. Huo, M. Wang, D. Zhang, T. Zhang, H. Wu, X. Rao, H. Meng, S. Yin, J. Mei, D. Zhang, X. Chen, J. Lv, M. Liu, Y. Cheng, Y. Guan, B. Feng, G. Song, C. Yi, M. Liu, F. Zeng, L. Wang, D. Li, Nat. Chem. Biol. 20 (2024) 1176–1187.
[22] L. Yang, L. Wang, Y. Huo, X. Chen, S. Yin, Y. Hu, X. Zhang, R. Zheng, H. Geng, H. Han, X. Ma, M. Liu, H. Li, W. Yu, M. Liu, J. Wang, D. Li, Mol. Ther. 28 (2020) 1673–1683.
[23] L. Villiger, H.M. Grisch-Chan, H. Lindsay, F. Ringnalda, C.B. Pogliano, G. Allegri, R. Fingerhut, J. Häberle, J. Matos, M.D. Robinson, B. Thöny, G. Schwank, Nat. Med. 24 (2018) 1519–1525.
[24] J.T. Bulcha, Y. Wang, H. Ma, P.W.L. Tai, G. Gao, Signal Transduct. Target. Ther. 6 (2021) 53.
[25] K. Paunovska, D. Loughrey, J.E. Dahlman, Nat. Rev. Genet. 23 (2022) 265–280.
[26] A.V. Anzalone, L.W. Koblan, D.R. Liu, Nat. Biotechnol. 38 (2020) 824–844.
[27] X. Huang, N. Kong, X. Zhang, Y. Cao, R. Langer, W. Tao, Nat. Med. 28 (2022) 2273–2287.
[28] J. Wang, H. Zhu, J. Gan, G. Liang, L. Li, Y. Zhao, Adv. Mater. 36 (2024).
[29] S. Xu, D. Liang, Q. Wang, Y. Cheng, D. Xie, Y. Gui, H. Zhang, C. Feng, F. Zhao, W. Ren, G. Sun, Y. Yang, L. Li, Y. Lai, B. Fu, Y. Lu, Z.J. Wang, Y. Wu, Nat Biomed Eng. (2025), https://doi.org/10.1038/s41551-025-01480-y.
[30] Y. Sun, S. Chatterjee, X. Lian, Z. Traylor, S.R. Sattiraju, Y. Xiao, S.A. Dilliard, Y. C. Sung, M. Kim, S.M. Lee, S. Moore, X. Wang, D. Zhang, S. Wu, P. Basak, J. Wang, J. Liu, R.J. Mann, D.F. LePage, W. Jiang, S. Abid, M. Hennig, A. Martinez, B. A. Wustman, D.J. Lockhart, R. Jain, R.A. Conlon, M.L. Drumm, C.A. Hodges, D. J. Siegwart, Science 384 (2024) 1196–1202.
[31] M. Kim, E.S. Song, J.C. Chen, S. Chatterjee, Y. Sun, S.M. Lee, S. Wu, P. Patel, Z. Tian, A. Kantor, B.A. Wustman, D.J. Lockhart, D.J. Siegwart, Nat. Biotechnol. (2025), https://doi.org/10.1038/s41587-025-02675-z.
[32] K. Musunuru, A.C. Chadwick, T. Mizoguchi, S.P. Garcia, J.E. DeNizio, C.W. Reiss, K. Wang, S. Iyer, C. Dutta, V. Clendaniel, M. Amaonye, A. Beach, K. Berth, S. Biswas, M.C. Braun, H.M. Chen, T.V. Colace, J.D. Ganey, S.A. Gangopadhyay, R. Garrity, L.N. Kasiewicz, J. Lavoie, J.A. Madsen, Y. Matsumoto, A.M. Mazzola, Y. S. Nasrullah, J. Nneji, H. Ren, A. Sanjeev, M. Shay, M.R. Stahley, S.H.Y. Fan, Y. K. Tam, N.M. Gaudelli, G. Ciaramella, L.E. Stolz, P. Malyala, C.J. Cheng, K. G. Rajeev, E. Rohde, A.M. Bellinger, S. Kathiresan, Nature 593 (2021) 429–434.
[33] S. Zhao, K. Gao, H. Han, M. Stenzel, B. Yin, H. Song, A. Lawanprasert, J.E. Nielsen, R. Sharma, O.H. Arogundade, S. Pimcharoen, Y.-J. Chen, A. Paul, J. Tuma, M. G. Collins, Y. Wyle, M.G. Cranick, B.W. Burgstone, B.S. Perez, A.E. Barron, A. M. Smith, H.Y. Lee, A. Wang, N. Murthy, Nat. Nanotechnol. 19 (2024) 1702–1711.
[34] R. Tenchov, J.M. Sasso, Q.A. Zhou, Bioconjug. Chem. 34 (2023) 941–960.
[35] M. Packer, D. Gyawali, R. Yerabolu, J. Schariter, P. White, Nat. Commun. 12 (2021) 6777.
[36] J. Lv, Y. Cheng, Chem. Soc. Rev. 50 (2021) 5435–5467.
[37] J. Lv, H. Wang, G. Rong, Y. Cheng, Acc. Chem. Res. 55 (2022) 722–733.
[38] Z. Zhang, X. Gao, Y. Li, J. Lv, H. Wang, Y. Cheng, CCS Chem. 5 (2023) 1411–1421.
[39] Y. Li, X. Yu, Q. Chen, H. Wang, J. Lv, Y. Cheng, Nano Today 56 (2024).
[40] Z. Zhang, W. Shen, J. Ling, Y. Yan, J. Hu, Y. Cheng, Nat. Commun. 9 (2018) 1377.
[41] J. Lv, Q. Fan, Y. Zhang, X. Zhou, P. Yu, X. Yu, C. Xin 2413006 (2025) 1–9.
[42] Y. yun Cheng, Acta Polym. Sin. 12 (2017) 1234–1245.
[43] T.L.M. Thurston, M.P. Wandel, N. Von Muhlinen, Á. Foeglein, F. Randow, Nature 482 (2012) 414–418.
[44] L.J. Jones, S.T. Yue, C.-Y. Cheung, V.L. Singer, Anal. Biochem. 265 (1998) 368–374.
[45] G.-H. Hwang, J. Park, K. Lim, S. Kim, J. Yu, E. Yu, S.-T. Kim, R. Eils, J.-S. Kim, S. Bae, BMC Bioinformatics 19 (2018) 542.